Describing the Relaxation Spectrum of Entangled Homopolymer Blends with the Dynamic Random-Phase Approximation

D. Lumma

Max-Planck-Institut für Polymerforschung, Ackermannweg 10, D-55128 Mainz, Germany

S. G. J. Mochrie*

Departments of Physics and Applied Physics, Yale University, New Haven, Connecticut 06520

Received May 19, 2000; Revised Manuscript Received June 27, 2001

ABSTRACT: Detailed calculations of the intermediate scattering function of entangled, binary homopolymer blends are presented. The calculations are based on the reptation model of polymer dynamics and employ the dynamic random-phase approximation for inferring collective blend behavior from single-chain characteristics. The relaxation spectra found here for blends—including the relaxation rates and amplitudes of higher-order modes—are contrasted with those for melts and are given for the entire range of length scales from the diffusive to the nondiffusive regime of polymer dynamics. Analytical limits of the intermediate scattering function are successfully compared to numerical results. The dominance of higher-order relaxation modes in specific, experimentally feasible, asymmetric blend systems is indicated, and the possibility of significant deviations of the expected time−correlation functions from a single-exponential decay is noted.

1. Introduction

Recent success in measuring the intermediate scattering function of an entangled homopolymer blend on microscopic length scales and over macroscopic time scales[1] suggests that the emerging technique of X-ray photon correlation spectroscopy (XPCS)[2−5] may soon advance far enough to yield results which may be compared to detailed theoretical predictions. Specifically, the XPCS measurements stimulating this article probe length scales comparable to or smaller than the radius of gyration of the component chains within a miscible polymer blend and access delay times within the viscous response of the transient network. The theoretical framework applicable to this region of dynamic phase space is the reptation model,[6,7] describing the relaxation spectrum of entangled polymer chains.

The reptation hypothesis[6,8] stipulates that a single polymer can be treated as confined within a tube with boundaries construed as the microscopic entanglements with the surrounding chains. These entanglements pose transient topological constraints on each chain,[9,10] forcing its dominant large-length-scale motion to be a creep along the tube's curvilinear path. The collective modes present in a blend of different species are taken to be expressed via the dynamic random-phase approximation (RPA).[11−13] The presence of different species introduces complexity to the phenomenology beyond that in melts, generally adding interactions between different chains and introducing a second set of spatial chain parameters, as well as a second microscopic time. To describe the static structure factor of multicomponent mixtures, the use of the RPA appears to be validated by experiment. Neutron-scattering experiments on selectively deuterated mixtures of homopolymers and block copolymers, for example, reveal partial structure factors and interaction parameters which are mutually consistent and in quantitative agreement with the predictions of the multicomponent static RPA.[14]

In this article, we revisit explicit theoretical predictions for the relaxation spectrum of an entangled, binary homopolymer system in the one-phase region, pointing out fundamental differences between the reptative relaxation spectra of melts and blends that have not previously been emphasized. Specifically, in the context of the dynamic RPA, we find that for each relaxation mode present in a melt, the relaxation spectrum of a binary blend contains an additional, collective relaxation mode. For certain, experimentally feasible blend parameters, higher-order modes are even seen to dominate the principal mode of the multiexponential relaxation spectrum.

In addition to reptation, we expect each polymer in a blend to undergo faster Rouse motions within its confining tube.[15] These modes relax compositional fluctuations at smaller distances and shorter times than likely can be studied with XPCS. The fast relaxational mechanism can, however, be probed via neutron-spin echo (NSE) measurements.[16] In such experiments, the intermediate scattering function is observed to display an initial short-time decay and then to approach a nonzero level of almost vanishing decay rate. This "plateau" persists to times at least as long as can be achieved with the NSE technique. The subsequent decay of the intermediate scattering function, inaccessible with NSE, can be characterized by means of XPCS. Coherent X-ray scattering and NSE should thus be considered complementary scattering techniques for probing the dynamic structure factor of entangled polymeric systems on microscopic length scales. Both experimental approaches can in principle access length scales that cannot easily be studied with dynamic light scattering. The numerical calculations presented in the present article were, in fact, used to model recently published XPCS data on compositional fluctuations in a homogeneous homopolymer blend of poly(ethylene oxide) and poly(methyl methacrylate).[1]

This article is organized as follows. In section 2, we review several key results concerning reptative dynamics. The intermediate scattering function and the susceptibility of a single chain are presented, the formalism of the dynamic RPA is introduced, and the overall

10.1021/ma000875y CCC: $20.00
Published on Web 10/12/2001

wavevector dependence of the reptative decay spectrum is discussed. In section 3, analytical approximations for the relaxational modes in blends are compared to numerically determined relaxation spectra and mode amplitudes in entangled, binary blends. There, we also briefly recall the question of how the slow and the fast component in a binary polymer blend interplay in controlling mutual diffusion. Experiments aiming to further address this issue by probing the intermediate structure factor are proposed. Section 4 presents the central result of this article—that it is possible for the intermediate scattering function in asymmetric blends to be dominated by higher-order modes. The strength of the higher-order modes is characterized throughout the parameter space of a polymer blend, and the experimental feasibility of a corresponding blend system is illustrated. The line shape of the resulting intensity autocorrelation function measured via photon correlation techniques is compared to that of a single-exponential decay. Section 5 concludes the present article by placing our results into the context of previous work and by summarizing the potential benefit of future XPCS measurements on entangled homopolymer blends.

2. Review of Previous Work

The complete intermediate scattering function of an entangled polymeric system, $f^{\text{net}}(Q, t)$, can be modeled as a superposition of distinct relaxation spectra. This superposition may be written in the form

$$f^{\text{net}}(Q, t) = A^{\text{rept}}(Q) f^{\text{rept}}(Q, t) + [1 - A^{\text{rept}}(Q)] f^{\text{rapid}}(Q, t) \quad (1)$$

The function $f^{\text{rept}}(Q, t)$ describes the reptative relaxation spectrum of a transient network of entangled chains. The function $f^{\text{rapid}}(Q, t)$, in contrast, describes the far more rapid relaxations due to motions on the segmental level of the chains. The underlying, fast modes belong to the Rouse spectrum.[15] Both functions satisfy the requirement that $f(Q, t \rightarrow 0) = 1$. The two relaxation spectra are governed by different fundamental time scales. As a consequence, the intermediate scattering function for an entangled polymer system reaches a wavevector-dependent "plateau" value at times larger than the characteristic Rouse relaxation time and smaller than the chain disentanglement time.

The quantity $A^{\text{rept}}(Q)$ in eq 1 denotes the wavevector-dependent amplitude of the reptative decay spectrum. We expect this quantity to decrease with increasing wavevector. The smaller the length scales probed, the more dominant the influence of the fast, segmental motion on the observed equilibrium fluctuations will be. In the framework of the classical reptation model, the mode amplitude of the curvilinear creep in *melts* is hypothesized to be given by

$$A^{\text{rept}} = \exp\left(-\frac{Q^2 d^2}{36}\right) \quad (2)$$

where d is the distance between entanglement points in the transient network.[7] The entanglement distance identifies the characteristic length scale on which the amplitude of the reptative decay spectrum, $A^{\text{rept}}(Q)$, becomes insignificant. For the more general case of blends, it remains unclear how to apply the tube concept, and no straightforward generalization of eq 2 to blends has been suggested so far.

This article is exclusively concerned with the properties of the function $f^{\text{rept}}(Q, t)$, which in the context of the reptation model is independent of the overall amplitude of the reptative decay, $A^{\text{rept}}(Q)$. Since $A^{\text{rept}}(Q)$ can in principle be measured independently, dynamic scattering experiments in the long-time regime may directly address the behavior of the reptative decay modes described by $f^{\text{rept}}(Q, t)$. In the following, we will simply refer to this function as $f(Q, t)$.

2.1. Time Domain and Laplace Space. The normalized intermediate scattering function of a system, $f(Q, t) = S(Q, t)/S(Q)$, where $S(Q)$ denotes the static structure factor, is related to the wavevector- and Laplace-frequency-dependent susceptibility, $\alpha(Q, p)$, via the fluctuation−dissipation theorem. Specifically, we have[17]

$$S(Q, t) = S(Q) \sum_m a_m(Q) \exp[-\Gamma_m(Q)t] \quad (3)$$

where the relaxation spectrum, $\Gamma_m(Q)$, is derived from

$$\alpha^{-1}[Q, p = -\Gamma_m(Q)] = 0 \quad (4)$$

and the mode amplitudes, $a_m(Q)$, are calculated as the residues corresponding to these pole singularities,

$$a_m(Q) = \frac{1}{S(Q)\Gamma_m(Q)} \text{Res}_{p=-\Gamma_m(Q)} \alpha(Q, p) \quad (5)$$

The mode amplitudes calculated in this article, $a_m(Q)$, are normalized to unity, $\sum_m a_m(Q) = 1$, which is equivalent to the condition that $f(Q, t \rightarrow 0) = 1$.

2.2. Single-Chain Intermediate Scattering Function. The simplest case of reptative dynamics occurs in a melt of monodisperse, entangled chains. To introduce its main features, and to allow generalization to the case of blends, we will address the description of such a system both in the time domain and in Laplace space. Correspondingly, we will provide expressions for the intermediate scattering function and the susceptibility of a single chain.

The intermediate scattering function of a single, labeled chain in a monodisperse melt of chemically identical chains has been calculated,[6] and is given by

$$S_0(Q, t) = \sum_{\substack{\text{all } \theta_m > 0, \\ \theta_m \tan\theta_m = \mu}} \frac{2\mu}{\theta_m^2(\mu^2 + \theta_m^2 + \mu)} \sin^2\theta_m \exp\left(-\frac{4\theta_m^2}{\pi^2}\frac{t}{\tau_d}\right) \quad (6)$$

where

$$\mu = \frac{1}{2}Q^2 R_g^2 \quad (7)$$

with R_g denoting the chains' radius of gyration. The variables θ_m refer to positive solutions of the equation

$$\theta_m \tan\theta_m = \mu \quad (8)$$

The variable m of eqs 6 and 8 labels the chain relaxation modes, and will hereafter be referred to as the "mode number". On the basis of the equations introduced so far, the index m could refer to an arbitrary sequence of labels. For the case of a monodisperse polymer melt,

however, the index m is sensibly chosen to refer to the sequence of odd integers, $m = 1, 3, 5, ...$, in light of the limiting cases discussed below.

The quantity τ_d in eq 6 denotes the so-called "disentanglement" time, the time necessary for a single chain to escape from the tube of its initial confinement. The corresponding relaxation rates are given by $\Gamma_m(Q) = 4\theta_m^2/(\pi^2\tau_d)$. We assume throughout this article that the static structure of the polymer molecules is well-described by the Gaussian-chain model, where $R_g^2 = N l^2/6$, with N the degree of polymerization and l the statistical segment length. The two chain characteristics R_g and τ_d define the fundamental length and time scales in which the dynamic phase space of the system's relaxation spectrum is naturally parametrized.

For comparison with the blend results presented below, we consider two limiting cases. For $\mu \ll 1$, eq 6 reduces to a single-exponential decay, with eq 8 leading to $\theta_1 \simeq \sqrt{\mu} \ll 1$. This implies a relaxation rate proportional to the square of the wavevector, $\Gamma_c = D_c Q^2$. The quantity D_c refers to the macroscopic diffusion constant and is given by $D_c = 2R_g^2/(\pi^2\tau_d)$. For $\mu \gg 1$, probing distances smaller than the coil radius, one finds that $\theta_m \simeq \pi/2 \times 1, 3, 5 ....$ Consequently, in this limit, the normalized intermediate scattering function reduces to

$$f_0(t) = \frac{8}{\pi^2} \sum_{\substack{m=1 \\ m \text{ odd}}}^{\infty} \frac{1}{m^2} \exp\left(-\frac{tm^2}{\tau_d}\right) \tag{9}$$

Equation 9 describes the so-called "nondiffusive" regime of polymer melt dynamics, where the reptative relaxation spectrum evident in the intermediate scattering function becomes independent of wavevector. In this regime, the melt relaxation rates are given by $\Gamma_m = m^2/\tau_d$, where m denotes an odd integer. In light of this limiting case, the mode numbers m for the melt case of eq 6 were assigned to be odd integers.

2.3. Single-Chain Susceptibility. The intermediate scattering function of eq 6 can be transformed to Laplace space, yielding the susceptibility[13]

$$a_0(Q, p) = \frac{1}{\mu^2 - \sigma^2}\left(\frac{\mu^2}{\sigma\mu \coth \sigma + \sigma^2} - \frac{1}{1 + \coth \mu}\right), \quad p > 0$$

$$= \frac{1}{\mu^2 + \sigma^2}\left(\frac{\mu^2}{\sigma\mu \cot \sigma - \sigma^2} - \frac{1}{1 + \coth \mu}\right), \quad p < 0 \tag{10}$$

where

$$\sigma = (\pi/2)\sqrt{|p|\tau_d} \tag{11}$$

The inverse Laplace transformation of eq 10 can be performed by applying eqs 3−5. Doing so requires determining the poles of the susceptibility $a_0(Q, p)$ and calculating the corresponding residues. As expected, this procedure recovers the intermediate scattering function in the time domain, given by eq 6.

The solid lines in Figure 1 show the relaxation spectrum of a monodisperse homopolymer melt. The relaxation rates, Γ_m for odd m, are shown as a function of the square of the wavevector, $Q^2R_g^2$, for mode numbers from 1 to 5. At large wavevectors, we observe a crossover toward a wavevector-independent relaxation rate. The corresponding mode amplitudes are shown in

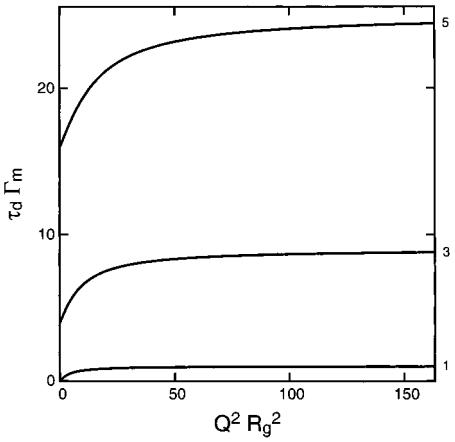

Figure 1. Relaxation spectrum, Γ_m, of an entangled, monodisperse homopolymer melt. The relaxation rates shown on the ordinate are normalized by the disentanglement time, τ_d, and are plotted vs the square of the normalized wavevector, $Q^2R_g^2$. Indices identify the mode number, m.

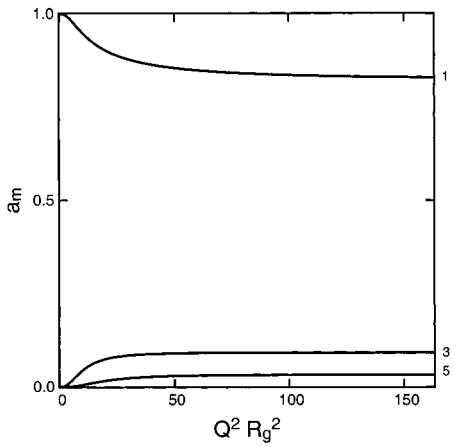

Figure 2. Mode amplitudes, a_m, for the case of a monodisperse homopolymer melt. The amplitudes for poles of different order are shown vs the square of the normalized wavevector, $Q^2R_g^2$. The indices identify the mode number, m.

Figure 2. We can find a crossover similar to the one evident in the relaxation rates. In the limit of probing length scales smaller than the coil sizes, for $Q^2R_g^2 \gg 1$, the mode amplitudes also approach wavevector-independent values which decrease with increasing mode number. In this nondiffusive regime of polymer dynamics, the weighted relaxation spectrum of the melt becomes independent of wavevector. The observed crossover is consistent with the two limiting cases mentioned above.

In the limit of probing large length scales ($Q^2R_g^2 \ll 1$), all higher-order poles ($m > 1$) approach zero weight, and the intermediate scattering function reduces to a single-exponential decay. The latter conclusion goes along with a Q^2 dependence of the relaxation rates at small wavevectors. At larger wavevectors, higher-order poles acquire nonzero weights, and the line shape in the time domain becomes multiexponential. Figures 1 and 2, in fact, display the results of a numerical procedure, which we have developed in order to calculate the mode relaxation rates and amplitudes in binary blends (see below). Applying this procedure to a melt, we may compare the numerical results at large wavevectors to eq 9. An example of such a comparison for $Q^2R_g^2 = 1200$ is shown in Figure 3, for both the mode relaxation rates and the mode amplitudes. Evidently, the numerical

calculations provide a good description of the analytical limit. In addition, eq 6 was compared numerically to the inverse Laplace transform of eq 10, leading to full agreement within numerical accuracy.

2.4. The Random-Phase Approximation. So far we have considered the single-chain response function. The dynamic RPA provides a procedure to model the effects of interactions and of the presence of multiple species. Specifically, the prescription for calculating the collective susceptibility $\bar{a}_0(Q, p)$ in a binary blend with only excluded volume interactions from the single-chain susceptibilities $a_{0i}(Q, p)$ is that[13]

$$\bar{a}_0(Q, p)^{-1} = v_0\{[\phi_1 v_1 N_1 a_{01}(Q, p)]^{-1} + [\phi_2 v_2 N_2 a_{02}(Q, p)]^{-1}\} \quad (12)$$

where ϕ_i, v_i, and N_i refer to the volume fraction, the volume of a statistical segment, and the number of statistical repeat units, respectively, of polymer species i. The quantity v_0 denotes the volume of an arbitrarily chosen reference monomer. Equation 12 could be employed for modeling the relaxation spectrum of a monodisperse, binary polymer blend without any interactions except for those due to excluded volume effects. Such a system may be approximated by a blend of chemically identical polymers containing one protonated and one deuterated fraction.

For a binary system composed of two chemically distinct polymers, the dynamic RPA introduces an interaction parameter, χ, to model the collective susceptibility of the interacting system, $\bar{\alpha}(Q, p)$. In terms of the susceptibility for the corresponding noninteracting system, $\bar{a}_0(Q, p)$, one obtains

$$\bar{\alpha}(Q, p) = \frac{\bar{a}_0(Q, p)}{1 - 2\chi\bar{a}_0(Q, p)} \quad (13)$$

where the interaction parameter is relative to the volume of the reference monomer, v_0. To model the collective susceptibility for a binary blend of chemically distinct polymers, eqs 12 and 13 can be combined, leading to

$$\bar{\alpha}(Q, p)^{-1} = v_0\left\{[\phi_1 v_1 N_1 a_{01}(Q, p)]^{-1} + [\phi_2 v_2 N_2 a_{02}(Q, p)]^{-1} - \frac{2\chi}{v_0}\right\} \quad (14)$$

This expression is applicable to monodisperse systems. In combination with eqs 3−5, the problem of calculating the blend's intermediate scattering function is reduced to finding the poles and the corresponding residues of eq 14.

3. Collective Dynamics of a Binary Blend

In the following section, analytical expressions for the collective relaxation spectrum in an entangled, binary blend are presented and compared to numerical calculations. The numerical results will describe the continuous crossover from the diffusive to the nondiffusive regime of polymer dynamics.

3.1. Analytical Results. In this section, we will consider the generalized susceptibility of a blend system in two regimes: in the limit of small wavevector ($Q^2R_{g1}^2 \ll 1$ and $Q^2R_{g2}^2 \ll 1$) and in the limit of large wavevector ($Q^2R_{g1}^2 \gg 1$ and $Q^2R_{g2}^2 \gg 1$). These conditions identify different dynamical regimes. We treat the case of a binary, monodisperse blend of two species with separate disentanglement times, differing spatial parameters, and arbitrary volume fractions. By considering the two limits mentioned, we will be able to reach our results analytically. Doing so provides us with an independent verification of the numerical findings discussed below. Moreover, the analytical results will allow us to conclude that all the relaxational modes in a blend are indeed of a collective nature, in that both the relaxation rates and the corresponding amplitudes depend on properties of both polymer species.

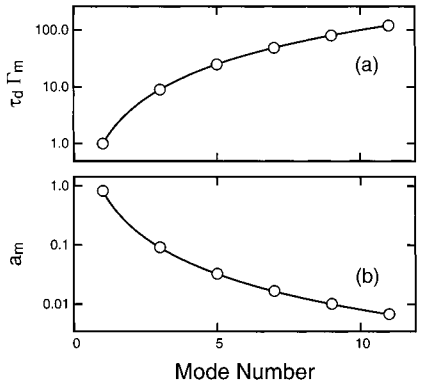

Figure 3. Melt dynamics in the limit of large wavevectors, $Q^2R_g^2 = 1200$. The open symbols show numerical results, while the solid lines illustrate the analytical limit of eq 9. Key: (a) normalized relaxation rates vs mode number, m; (b) amplitude vs mode number. Note that relaxational modes in a melt only occur at odd integer mode numbers. The solid curves are a continuation of the m dependences seen in eq 9.

We now consider eq 14 in the limit of small wavevector, defined by $\mu_1 \ll 1$ and $\mu_2 \ll 1$. With the further assumptions that $\mu_1 \ll \sigma_1$, $\mu_2 \ll \sigma_2$, $\sigma_1 \ll 1$, and $\sigma_2 \ll 1$, one obtains

$$\bar{\alpha}(Q, p)^{-1} \simeq \left(\frac{v_0}{\phi_1 v_1 N_1} + \frac{v_0}{\phi_2 v_2 N_2} - 2\chi\right) - \frac{\pi^2}{2Q^2}\left(\frac{\tau_{d1}}{\phi_1 v_1 N_1 R_{g1}^2} + \frac{\tau_{d2}}{\phi_2 v_2 N_2 R_{g2}^2}\right)p \quad (15)$$

This susceptibility gives rise to a single-exponential intermediate scattering function with a relaxation rate

$$\Gamma_c = D_c Q^2 = \frac{(\phi_1 v_1 N_1)^{-1} + (\phi_2 v_2 N_2)^{-1} - 2\chi/v_0}{(\phi_1 v_1 N_1 D_1)^{-1} + (\phi_2 v_2 N_2 D_2)^{-1}} Q^2 \quad (16)$$

where $D_1 = 2R_{g1}^2/(\pi^2\tau_{d1})$, and $D_2 = 2R_{g2}^2/(\pi^2\tau_{d2})$. Evidently, the decay of the intermediate scattering function is diffusive, with a collective diffusion coefficient D_c.

It is important to note that eq 10, and consequently eqs 14 and 16, implicitly assume that reptation occurs in a matrix of fixed obstacles and that the blend system is incompressible. Brochard considered collective diffusion in the case that reptation occurs in a moving tube[18] and obtained the collective diffusion coefficient in the limit of small wavevectors as

$$D_{c\,\mathrm{Brochard}} = \left(\frac{1}{\phi_1 v_1 N_1} + \frac{1}{v_2\phi_2 N_2} - \frac{2\chi}{v_0}\right)\phi_1\phi_2 \times (\phi_1 v_1 N_1 D_1 + \phi_2 v_2 N_2 D_2) \quad (17)$$

The predictions of eq 16 and eq 17 are quite different.

Equation 16 implies that the slower component among the two controls the collective diffusion coefficient. By contrast, eq 17 predicts that the faster component among the two will dominate.

Semenov argues that intuitive arguments can be given which support either one of these two, contradictory results.[19] The "fast diffusion idea", according to Semenov, is based on the notion that the fast chain component would be capable of rapidly diffusing into a matrix of the slower chain component. The faster component would thus drive the process of mixing, and thereby relax any compositional fluctuations, dominating collective diffusion. Semenov also describes the notion underlying the "slow diffusion idea". One might reason, he points out, that any reptative motion of fast chains into a matrix of slower chains necessitates that the slow molecules move elsewhere first. The incompressibility of the system would force the faster chains to remain at their positions until the slower ones had freed space for them. The process would then be dominated by the slower chain component.

The question of whether the fast or the slow component in a blend of two dynamically distinct polymer species dominates mutual diffusion has a long history in polymer science. It had seemed for some time as if the available experimental evidence favored the dominance of the fast component.[20−22] More recently, however, Shearmur and co-workers, in an article that also provides a review of the present state of the discussion, have argued that both the "slow" and the "fast" theory are valid, yet are applicable to different dynamic regimes.[23] They reason that at lower temperatures, just slightly above the blend's glass transition temperature, only a small amount of free volume is available, and the condition of incompressibility is met closely. This condition is an assumption crucial to the "slow theory". At higher temperatures, they reason, free volume vacancies are more likely to appear, which may then lead to localized inhomogeneities in density. The existence of such inhomogeneities is featured as a fundamental assumption in many derivations of the "fast theory".

Consequently, Shearmur and co-workers conclude that the "slow theory" should be expected to apply at lower temperatures and the "fast theory" at higher temperatures. In support of their reasoning, they also provide data from nuclear reaction analysis on low-molecular-weight blends of polystyrene and poly(methyl methacrylate). In addition, they provide an explanation for why most available evidence so far, as cited in their article, has supported the dominance of the fast component in entangled blends: in order to yield diffusion at experimentally accessible diffusion rates, studies on long chains tended to perform measurements far above the glass transition temperature, and the data would thus, according to Shearmur and co-workers, have ended up favoring the "fast theory".

Any such reasoning will remain speculative until systematic measurements of the collective diffusion constant have been performed. Those could be carried out on a monodisperse, binary blend system with a well-characterized static scattering cross section. The system would preferably consist of two long-chain components with distinct disentanglement times. Measurements of the relaxation rate as a function of wavevector and composition, $\Gamma_c(Q,\phi_1)$, would then yield the collective diffusion coefficient, $D_c(\phi_1)$, in the limit of small wavevectors. The latter could be directly compared to eqs 16 and 17. Recent experiments on blends of poly(ethylene oxide) [PEO] and poly(methyl methacrylate) [PMMA] suggest that measurements of this kind are technically feasible by means of XPCS.[1] The measurements were performed at the lowest sensible temperature of 70 °C, slightly above the crystallization temperature of PEO and below the glass transition temperature of PMMA, leading to disentanglement times on the order of tens of seconds. These XPCS data may reasonably be expected to belong to the low-temperature regime described by Shearmur and co-workers, within which mutual diffusion would be dominated by the slow component. However, to establish definitively to which regime these data belong, further experiments would be needed. The calculations in the present article were used as a model for these XPCS measurements, and are based on the "slow theory" exclusively. It is well-known that the PMMA chains in PEO−PMMA blends exhibit far smaller relaxation rates than the PEO chains.[24] This, if any, experimental situation is the one that most closely resembles the motion of one chain species through a web of fixed obstacles, an assumption underlying eqs 10, 14, and 16. Lodge and co-workers point out that such a situation corresponds to one case in which linear chains might indeed execute a form of strict reptation: sufficiently long chains of one species relax within an essentially static network of other chains.[25]

According to eq 14, with increasing wavevectors the role of the interaction parameter, χ, becomes progressively less important in determining the mode structure. Thus, in the limit $Q^2R_{g1}^2 \gg 1$, $Q^2R_{g2}^2 \gg 1$, we may neglect χ. Further assuming $\sigma_1 \ll \mu_1$ and $\sigma_2 \ll \mu_2$, eq 15 becomes

$$\bar{a}_0(Q, p)^{-1} \simeq \frac{Q^2 v_0}{12}(x_1\sigma_1 \cot \sigma_1 + x_2\sigma_2 \cot \sigma_2) \quad (18)$$

where $x_1 = l_1^2/(\phi_1 v_1)$and $x_2 = l_2^2/(\phi_2 v_2)$, with l_1 and l_2 denoting the statistical segment lengths of the two chain species.

Since the wavevector appears in eq 18 only as an overall factor, the predicted relaxation rates and mode amplitudes are independent of wavevector. We thus recover the result found for single-chain reptative relaxation, that the relaxation of equilibrium fluctuations becomes independent of wavevector when probing length scales significantly smaller than the component radii of gyration. This is a key result of the reptation model: on length scales smaller than the coil size, but greater than the distance between entanglements, relaxation occurs no faster than the disentanglement time, irrespective of wavevector. Within the framework of the model, this result can be understood intuitively. For a density fluctuation on a length scale in the described range to relax, the entire chain must reptate out of its tube of initial confinement. According to the classical reptation model, this process will always require a time interval corresponding to the disentanglement time, independent of the actual length scale on which the density fluctuation occurred.

A discrepancy with the classical reptation model is found in the N dependence of the viscosity of long-chain polymers, which is experimentally observed to vary as $N^{3.4}$. This result stands in contrast to the prediction of the classical reptation model,[26] according to which both the viscosity and the disentanglement time should vary as N^3. There have been several attempts to reconcile

the experimentally observed exponent with theoretical predictions.[25] It is generally believed that the discrepancy originates in the existence of a relaxation process which is faster than reptation but which becomes less important as N becomes larger. A candidate for such a process are the contour length fluctuations of the chain, during which the ends of a polymer are pulled back into its confining tube. Recently, this idea has been made concrete by constructing a quantitative theory of stress relaxation in long-chain polymers that contains relaxation modes due to both reptation and contour length fluctuations.[27] This theory predicts a viscosity that scales with $N^{3.4}$ over a large range of N, crossing over to a cubic dependence at very large N. Such contour length fluctuations, or other processes outside of the classical reptation model, may modify that model's prediction of a wavevector-independent decay rate on length scales smaller than the coil size.

The decay of the intermediate scattering function in eq 18 involves an infinite, discrete spectrum of exponential relaxations, each one corresponding to a different pole of eq 18. Specifically, there are modes with decay rates approximately given by

$$\Gamma_{m\ \mathrm{odd}} \simeq m^2\left(\frac{x_1\sqrt{\tau_{\mathrm{d}1}}+x_2\sqrt{\tau_{\mathrm{d}2}}}{x_1\tau_{\mathrm{d}1}+x_2\tau_{\mathrm{d}2}}\right)^2 \qquad (19)$$

$$\text{for } m = 1, 3, 5, \ldots,$$

and

$$\Gamma_{m\ \mathrm{even}} \simeq m^2\left[\frac{x_1\sqrt{\tau_{\mathrm{d}1}}+x_2\sqrt{\tau_{\mathrm{d}2}}}{(x_1+x_2)\sqrt{\tau_{\mathrm{d}1}}\sqrt{\tau_{\mathrm{d}2}}}\right]^2 \qquad (20)$$

$$\text{for } m = 2, 4, 6, \ldots$$

with the same notation as used above. For the corresponding mode amplitudes, we obtain

$$a_{m\ \mathrm{odd}} \simeq \frac{1}{m^2}\frac{8}{\pi^2}(x_1+x_2)\frac{x_1\tau_{\mathrm{d}1}+x_2\tau_{\mathrm{d}2}}{(x_1\sqrt{\tau_{\mathrm{d}1}}+x_2\sqrt{\tau_{\mathrm{d}2}})^2} \qquad (21)$$

$$\text{for } m = 1, 3, 5, \ldots$$

and

$$a_{m\ \mathrm{even}} \simeq 2x_1x_2\left(\frac{\sqrt{\tau_{\mathrm{d}1}}-\sqrt{\tau_{\mathrm{d}2}}}{x_1\sqrt{\tau_{\mathrm{d}1}}+x_2\sqrt{\tau_{\mathrm{d}2}}}\right)^2 \qquad (22)$$

$$\text{for } m = 2, 4, 6 \ldots$$

where we have used, in the large-wavevector limit, that the static cross section of the system reduces to

$$\bar{S}(Q)^{-1} \simeq \frac{Q^2v_0}{12}(x_1+x_2) \qquad (23)$$

Equations 19−22 are applicable only if the two disentanglement times do not deviate significantly from their common mean. To overcome this restriction, in a later section we will turn to numerical methods. When $x_1 = x_2$ and $\tau_{\mathrm{d}1} = \tau_{\mathrm{d}2}$, the amplitudes of eqs 21 and 22 reduce to $a_{m\ \mathrm{odd}} = 8/(\pi^2m^2)$ and $a_{m\ \mathrm{even}} = 0$. At the same time, the relaxation rates of the odd-numbered modes simplify to $\Gamma_{m\ \mathrm{odd}} \simeq m^2/\tau_{\mathrm{d}}$, and the melt case described by eq 9 is recovered.

For a blend, the even-numbered mode amplitudes of eq 22 do not exhibit a dependence on mode number. Given the infinite number of even-numbered modes, this result inevitably contradicts the requirement that the mode amplitudes a_m of eq 3 sum to unity. This inconsistency can be reconciled by noting that eq 22 was derived by an expansion of σ_1, σ_2 about even multiples of π. With increasing mode number, the deviation of σ_1, σ_2 from even multiples of π becomes more significant, and eq 22 loses its validity. Consequently, we expect eq 22 to hold for a limited number of modes only. All the relaxation rates and amplitudes obtained are dependent on the material constants of both species, signifying the collective nature of all modes considered here. How the considerations described by Brochard[18] might affect the large-wavevector dynamics has not to our knowledge been considered. Thus, whether eqs 19−22 survive such a change or how they may be modified remain open questions.

3.2. Numerical Results. Thus far, we have only considered blend relaxation in the limits of small and large wavevectors. To expand the scope of our investigation to wavevectors located in the crossover region between these two extremes, and to consider arbitrary deviations between the disentanglement times of the two blend species, we turn to the numerical procedure mentioned above. The calculations were performed by a computer algorithm written in the interpreted Yorick language,[28] and executed on a Sun Ultra 1 workstation. Both melt and blend systems could be modeled by the same routine. The melt case was simulated by defining a binary blend of two equal components.

To discuss the blend relaxation spectrum, it is instructive to consider first the simplest case of a binary, monodisperse homopolymer blend. The latter is given by a symmetric blend, for which both species occupy equal volume fractions, $\phi_1 = 1 - \phi_2 = {}^1/_2$. Furthermore, the two chain species involved are supposed to be spatially equivalent, exhibiting identical degrees of polymerization, specific volumes, and persistence lengths, implying equal radii of gyration, $R_{\mathrm{g}} = R_{\mathrm{g}1} = R_{\mathrm{g}2}$. Similarly, the two species were assumed not to interact other than via their excluded volume, corresponding to $\chi = 0$. The only distinction between the two polymer species is taken to be a difference in the two disentanglement times, given by $\tau_{\mathrm{d}1} = \tau_{\mathrm{d}}(1+\epsilon)$ and $\tau_{\mathrm{d}2} = \tau_{\mathrm{d}}(1-\epsilon)$ for polymer species 1 and 2, respectively. For the present calculations, we have chosen $\epsilon = 0.01$.

As we will illustrate in section 4.4, a blend of this kind is experimentally feasible. At the same time, the simplicity of this model system allows one to focus on the fundamental differences between the spectral structure of blend relaxation and that of melt relaxation. The structure of the blend relaxation spectrum is shown in Figure 4. The solid lines represent the relaxation rates of odd-numbered modes, while the dashed lines represent those for even-numbered modes. The relaxation rates of the odd-numbered modes are monotonically increasing with wavevector. Those of the even-numbered modes, in contrast, feature a local maximum which shifts toward larger wavevectors with increasing mode number.

At small wavevectors, each even-numbered mode appears to emerge from the next higher, odd-numbered mode. With increasing wavevector, all modes redistribute without the occurrence of any "mode crossings". The first mode is distinct from the higher-order, odd-numbered modes in that no other relaxations seem to emerge from it. Figure 4 raises the question of how the

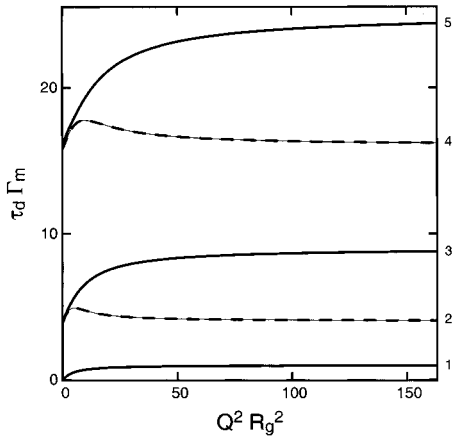

Figure 4. Relaxation spectrum, Γ_m, of an entangled, symmetric, binary blend of monodisperse chains in the one-phase region. The modeled system is a symmetric blend, $\phi_1 = 1 - \phi_2 = {}^1/_2$, with two chain species of equal radius of gyration, $R_g = R_{g1} = R_{g2}$. The disentanglement times are given by $\tau_{d1} = \tau_d(1 + \epsilon)$ and $\tau_{d2} = \tau_d(1 - \epsilon)$ for polymer species 1 and 2, respectively, with $\epsilon = 0.01$. The interaction between the two species is assumed to be zero, $\chi = 0$. The relaxation rates shown on the ordinate are normalized by the average disentanglement time, τ_d, and are plotted vs the square of the normalized wavevector, $Q^2R_g^2$. The indices identify the mode number, m. The solid lines indicate the relaxation rates of the odd-numbered poles, while the dashed lines identify those of the even-numbered poles.

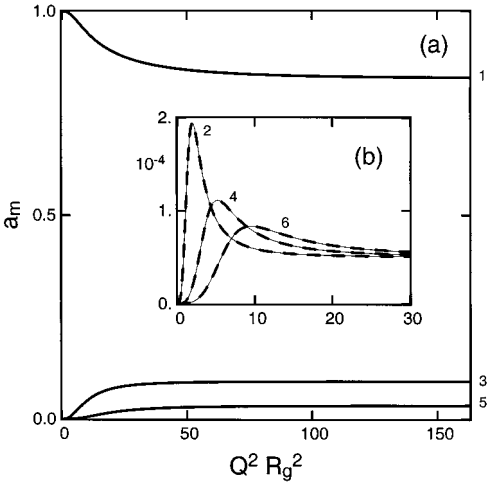

Figure 5. Mode amplitudes, a_m, for the same symmetric binary blend considered in Figure 4. Key: (a) amplitudes for odd-numbered poles vs normalized wavevector, $Q^2R_g^2$; (b) amplitudes for even-numbered poles vs normalized wavevector, $Q^2R_g^2$. The small indices identify the pole number, m.

two spectra for melt and blend case can differ so fundamentally, given that the corresponding physical systems are very similar. This is elucidated in Figure 5, which shows the normalized mode amplitudes. For these parameters, the first mode has the largest amplitude over the entire range of wavevectors, but its weight decreases monotonically with increasing wavevector. In the limit of small wavevectors, all higher-order modes ($m > 1$) assume zero weight. The relaxation spectrum then reduces to a single-exponential decay, as in the melt case. Also similar to the melt, the spectrum becomes independent of wavevector for large wavevectors.

In Figure 5, the mode amplitudes for the odd-numbered modes are separated from those of the even-numbered modes. We see that the even-numbered mode amplitudes share the feature of a local maximum, which becomes less pronounced and moves toward larger wavevectors with increasing mode number. Striking, here, is the absolute magnitude of the weights for the even-numbered modes, which is negligible compared to that of the odd-numbered modes. This finding reconciles the difference between melt and blend relaxation spectrum with the minor difference in the physical systems modeled. When we increase the ϵ-parameter from zero to finite values, the even-numbered modes appear in the relaxation spectrum. However, their relative statistical weight remains insignificant for small values of ϵ. As a result, the relative change to the intermediate scattering function of eq 3, which represents the physical quantity actually measured in experiments, remains negligible when tuning the ϵ-parameter from 0 to 0.01. Considering this effect, we conclude that the relaxation spectrum indeed changes discontinuously when ϵ is increased from zero. The intermediate scattering function, however, changes gradually, in accordance with physical intuition.

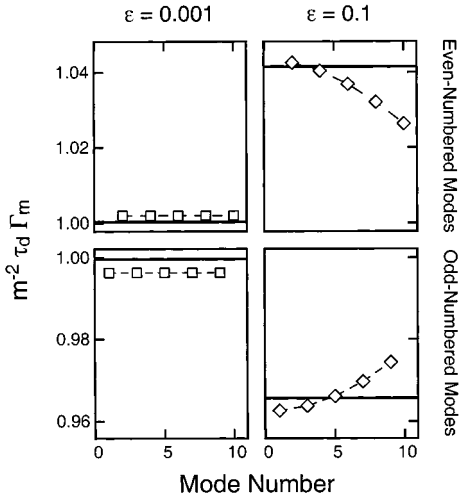

Figure 6. Normalized relaxation rates, $\tau_d\Gamma_m/m^2$, in the limit of large wavevectors, $Q^2R_g^2 = 1200$. Modeled is a binary, homopolymer blend with negligible interactions, $\chi = 0$. The two species are taken to occupy relative sample volumes of ${}^1/_3$ and ${}^2/_3$. The disentanglement times of the two species are given by $\tau_{d1} = \tau_d(1 + \epsilon)$ and $\tau_{d2} = \tau_d(1 - \epsilon)$ for polymer species 1 and 2, respectively. The open symbols represent numerical results from eq 12, while the solid lines indicate our analytical results for this regime. All data are shown for both even- and odd-numbered modes, and for two different values of the ϵ-parameter.

3.3. Comparison between Analytical and Numerical Results. In Figures 6 and 7, we compare our analytical inferences with the results of the numerical calculations based on eq 12. To do so, we consider a binary homopolymer blend. Since our analytical expressions simplify significantly in the case that $x_1 = x_2$, we must avoid considering a symmetric blend for this comparison. Instead, we treat a blend in which all spatial parameters of the two species are identical, but in which the volume fractions occupied by the two species vary. Specifically, we choose $\phi_1 = 1 - \phi_2 = {}^1/_3$. Moreover, the disentanglement times of the two species are chosen to be $\tau_{d1} = \tau_d(1 + \epsilon)$ and $\tau_{d2} = \tau_d(1 - \epsilon)$ for polymer species 1 and 2, respectively.

The resulting relaxation rates are shown in Figure 6, which allows comparison of numerical and analytical results, for both even- and odd-numbered modes, and for two different values of the ϵ-parameter. The relax-

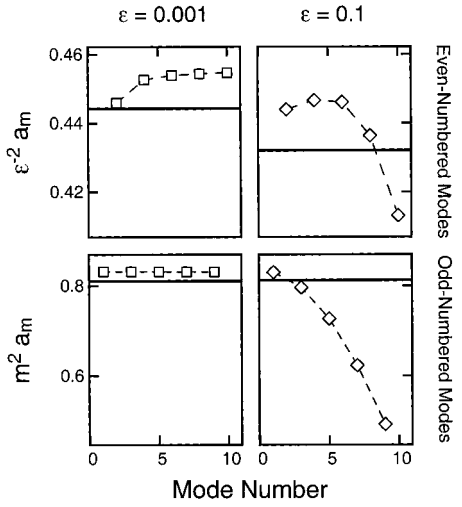

Figure 7. Normalized mode amplitudes, a_m, in the limit of large wavevectors, $Q^2R_g^2 = 1200$. Modeled is the same binary blend system considered in Figure 6. The open symbols represent numerical results from eq 13, while the solid lines indicate our analytical results for this regime. The even-numbered mode amplitudes are presented after correction for an expected ϵ^2 dependence, showing $\epsilon^{-2}a_m$. The odd-numbered mode amplitudes are normalized by the square of the mode number, showing m^2a_m. All data are presented for two different values of the ϵ-parameter.

ation rates are normalized by the mean disentanglement time, τ_d, and by the predicted m^2 dependence. For $\epsilon \leq 0.01$, we indeed observe this dependence in our numerical results, in both odd- and even-numbered modes. (Only data for $\epsilon = 0.001$ are shown.) The relaxation rates of the even-numbered modes are underestimated, while those of the odd-numbered modes are overestimated by our analytical approximations. For $\epsilon = 0.001$, however, the deviations between numerical and analytical data are smaller than 1%. For $\epsilon = 0.1$, in contrast, a systematic deviation of the numerical results from the analytical approximations is evident, for both even- and odd-numbered modes. This finding indicates that our analytical approximations break down for larger deviations between the disentanglement times of the two polymers. This was to be expected since our derivation of the analytical approximations involved expanding the susceptibility in terms of the deviations of σ_1, σ_2 from their mean. For large ϵ-parameters, however, this expansion ceases to be accurate.

Similar results hold true when considering the corresponding mode amplitudes of Figure 7. For ϵ-parameters up to 0.01, the deviation between numerical and analytical results lies below 4%. (Only data for $\epsilon = 0.001$ are shown.) For $\epsilon = 0.1$, in contrast, we see larger, systematic deviations, especially for higher mode numbers. It is particularly important to note the strong decrease in the amplitude of the even-numbered modes with mode number, m. This decrease stresses the limited validity of the m-independent behavior predicted by our analytical calculations for the even-numbered modes. It may be noted that for small ϵ-parameters, eq 22 leads to $a_{m\,\mathrm{odd}} \propto \epsilon^2$, a behavior that is reflected by the absolute magnitudes of the even-numbered mode amplitudes in Figure 7.

4. Dominant Higher-Order Modes in the Nondiffusive Regime

For symmetric binary blends, where $\phi_1 = \phi_2$, we have shown that the relative amplitude of the odd-numbered modes decreases roughly with the square of the mode number, m^2. The even-numbered mode amplitudes, in contrast, show a far less sensitive dependence on mode number, at least for small mode numbers, and their absolute magnitude remains small in comparison to that of the odd-numbered modes. This situation changes in the general case of asymmetric blends, where the amplitude of the even-numbered modes can become appreciable.

In binary blends, the two chain components may generally differ in any of their fundamental parameters. In the present theoretical framework, these parameters comprise the chains' radius of gyration as well as their disentanglement time. In the following, we will independently consider the two cases in which the two blend components differ in their respective radii of gyration or in their disentanglement times. Given that the present manuscript focuses on the dynamics in the nondiffusive regime, it will turn out that the relaxation spectra of blends containing components with different disentanglement times are most interesting, and we will therefore thoroughly explore their behavior as a function of composition. In this context, we present a specific, asymmetric blend system in which higher-order modes dominate the intermediate scattering function of the blend. This finding, which we consider the most important result of this article, is the more interesting since it applies to a blend system with experimentally feasible parameters. First, however, we present results for a blend of components with different radii of gyration.

4.1. Blends of Components with Different Radii of Gyration. When considering a homopolymer blend consisting of component chains with different radii of gyration, one effectively introduces a second spatial scale to the kind of blend that was discussed in the previous section. The consequences of this change in the limits of small and large wavevectors become evident in the analytical expressions derived in section 3.1, especially eqs 16 and 19−22. The spectra both in the diffusive and in the nondiffusive regimes are not affected qualitatively when the two radii of gyration are assumed to differ. It is, however, to be expected that the wavevector dependence at intermediate scattering wavevectors of the relaxation spectrum will reflect the second spatial scale now present in the system.

This dependence is explored further in Figures 8 and 9, which describe an entangled, binary blend of monodisperse chains in the one-phase region. The modeled system is a symmetric blend, $\phi_1 = 1 - \phi_2 = {}^1/_2$, with two chain species of equal disentanglement times, $\tau_{d1} = \tau_{d2}$, and an interaction parameter between the two species that is assumed to be zero, $\chi = 0$. Figure 8 shows the relaxation spectrum for the cases that the two radii of gyration differ according to (a) $R_{g2} = 2R_{g1}$ and (b) $R_{g2} = 4R_{g1}$. The numerical data are plotted as a function of the normalized wavevector, $Q^2R_g^2$. The quantity R_g denotes the volume-averaged, mean-square radius of gyration, $R_g^2 = \sum_i \phi_i R_{gi}^2$. The two panels of Figure 8 do indeed confirm the expectation that the second spatial scale affects the wavevector dependence of the spectrum at intermediate wavevectors. Panel (a) of Figure 8 illustrates how the difference between the radii of gyration leads to the development of a shoulder in the wavevector dependence of the relaxation rate. For an even larger deviation among the two spatial scales, this shoulder turns into a local maximum, as is illustrated in panel (b). These findings are complemented by the

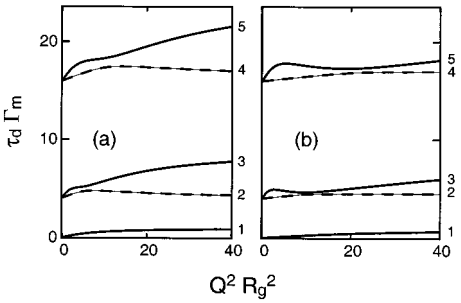

Figure 8. Relaxation spectrum, Γ_m, of an entangled, binary blend of monodisperse chains in the one-phase region. The modeled system is a symmetric blend, $\phi_1 = 1 - \phi_2 = {}^1/_2$, with two chain species of equal disentanglement times, $\tau_{d1} = \tau_{d2}$. The component radii of gyration vary according to (a) $R_{g2} = 2R_{g1}$ and (b) $R_{g2} = 4R_{g1}$. The interaction between the two species is assumed to be zero, $\chi = 0$. The relaxation rates shown on the ordinate are normalized by the average disentanglement time, τ_d, and are plotted vs the square of the normalized wavevector, $Q^2R_g^2$, where R_g denotes the volume-averaged, mean-square radius of gyration, $R_g^2 = \sum_i \phi_i R_{gi}^2$. The indices identify the mode number, m. The solid lines indicate the relaxation rates of the odd-numbered poles, while the dashed lines identify those of the even-numbered poles.

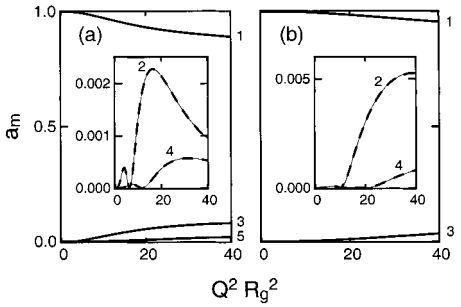

Figure 9. Mode amplitudes, a_m, for an entangled, homogeneous, binary blend, with component radii of gyration varying according to (a) $R_{g2} = 2R_{g1}$ and (b) $R_{g2} = 4R_{g1}$. The system modeled is the same as the one considered in Figure 8. Amplitudes are plotted vs the square of the normalized wavevector, $Q^2R_g^2$, where R_g denotes the volume-averaged, mean-square radius of gyration, $R_g^2 = \sum_i \phi_i R_{gi}^2$. The indices identify the mode number, m. The solid lines indicate the amplitudes of the odd-numbered poles, while the dashed lines in the insets identify those of the even-numbered poles.

corresponding mode amplitudes shown in Figure 9. Panels (a) and (b) show data describing the same model blends as in the previous figure. The solid lines represent the odd-numbered modes, while the dashed lines in the insets represent the even-numbered modes. The presence of a second spatial scale is apparently most visible in the oscillations of the even-numbered mode amplitudes. The wavevector dependence of the odd-numbered mode amplitudes seems qualitatively unchanged from their behavior in the case that both radii of gyration are equal.

The presence of a second spatial scale in a blend system, while clearly being reflected in the relaxation spectrum at intermediate wavevectors, does not seem to affect the structure of the spectrum in the nondiffusive regime, where the relaxation rates become independent of wavevector. The structure of the blend relaxation spectrum at small wavevectors, where collective relaxations become apparent, is similarly unaffected. What we have, however, not explored numerically until now are cases in which different disentanglement times are present in the blend. This is the topic of the following section.

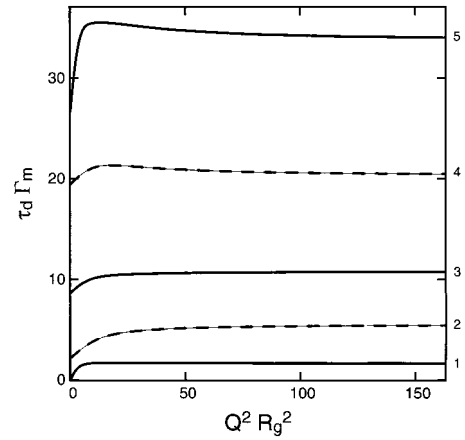

Figure 10. Relaxation spectrum, Γ_m, for an entangled, homogeneous, binary blend with dominant higher-order modes. The modeled system is an asymmetric blend, $\phi_1 = 1 - \phi_2 = 0.89$, with two monodisperse chain species of equal radius of gyration, $R_g = R_{g1} = R_{g2}$. The disentanglement times were chosen to differ appreciably between the two species, according to $\tau_{d1} = 12.3$ and τ_{d2} ($\epsilon = 0.85$). The interaction between the two species was assumed to be zero, $\chi = 0$. The relaxation rates shown on the ordinate are normalized by the average disentanglement time, τ_d, and are plotted vs the square of the normalized wavevector, $Q^2R_g^2$. The indices identify the mode number, m. The solid lines indicate the relaxation rates of the odd-numbered poles, while the dashed lines identify those of the even-numbered poles.

4.2. Blends of Components with Different Disentanglement Times. We consider a monodisperse, binary homopolymer blend with negligible interactions, where the interaction parameter is taken to equal zero, $\chi = 0$. The modeled system is an asymmetric blend, $\phi_1 = 1 - \phi_2 = 0.89$, with two monodisperse chain species of equal radius of gyration, $R_g = R_{g1} = R_{g2}$. The disentanglement times were chosen to differ appreciably (but not implausibly) between the two species. Specifically, we have chosen $\tau_{d1} = 12.3\tau_{d2}$, which corresponds to $\epsilon = 0.85$. The resulting relaxation spectrum is displayed in Figure 10, where the relaxation rates shown on the ordinate are normalized by the average disentanglement time, τ_d, and are plotted vs the square of the normalized wavevector, $Q^2R_g^2$. The solid lines indicate the relaxation rates of the odd-numbered poles, while the dashed lines identify those of the even-numbered poles.

There are significant differences between Figure 10 and the relaxation spectrum of Figure 4 for a symmetric blend. In the asymmetric case considered, we find no apparent pairing of modes at small wavevectors. As expected, the relaxation rates lack the regularity we found for the spectrum presented in Figure 4. In the asymmetric system, for instance, we find a relaxation rate with a local maximum vs wavevector among the odd-numbered modes, as well as a monotonically increasing relaxation rate among the even-numbered modes. More remarkable is Figure 11, which presents the corresponding mode amplitudes for our specific asymmetric blend. While the first mode dominates in the limit of small wavevectors, the amplitude of the second mode dominates the relaxation spectrum for large wavevectors. In the former limit, we observe the same behavior found previously: the first mode amplitude assumes the value of unity, and the relaxation spectrum reduces to a single-exponential decay. Consequently, the intermediate scattering function will reflect a crossover from a single-exponential decay

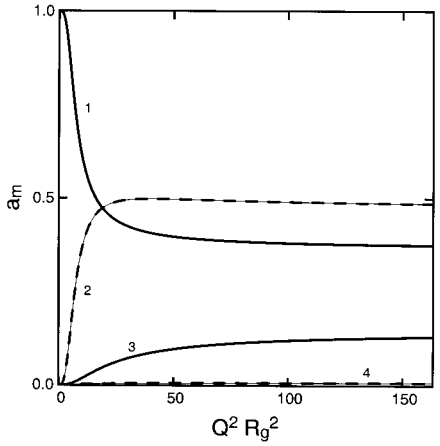

Figure 11. Mode amplitudes, a_m, for an entangled, homogeneous, binary blend with dominant higher-order modes. The system modeled is the same as the one considered in Figure 10. Amplitudes are plotted vs the square of the normalized wavevector, $Q^2R_g^2$. The indices identify the mode number, m. The solid lines indicate the amplitudes of the odd-numbered poles, while the dashed lines identify those of the even-numbered poles.

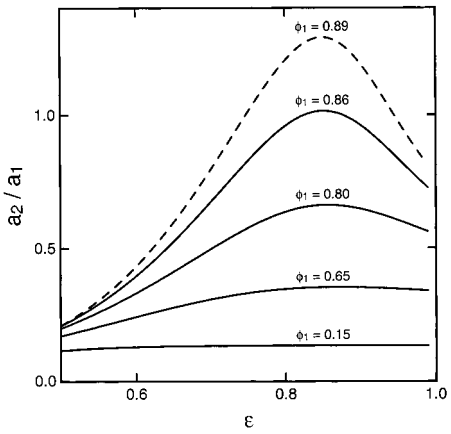

Figure 12. Multiexponentiality of the blend intermediate scattering function in the regime of large wavevectors, $Q^2R_g^2 = 1200$. The model describes a binary, monodisperse homopolymer blend in which both species consist of spatially equivalent chains. The disentanglement times of the two species are determined according to $\tau_{d1} = \tau_d(1 + \epsilon)$ and $\tau_{d2} = \tau_d(1 - \epsilon)$ for polymer species 1 and 2, respectively. The volume fractions are given by ϕ_1 and $\phi_2 = 1 - \phi_1$. Shown is the ratio a_2/a_1 as a function of the ϵ-parameter. The different curves refer to model blends with varying compositions.

spectrum governed by the first mode to a multiexponential decay dominated by the second mode.

4.3. The Significance of Blend Parameters for Higher-Order Modes. In the regime of small wavevectors, the dynamics of any entangled blend reduces to a single-exponential decay. At larger wavevectors, the relaxation spectrum is expected to become multiexponential. An assessment of multiexponentiality is therefore naturally carried out in the regime of large wavevectors. As was demonstrated in the previous section, there exist blend systems in which higher-order modes gain prominence in the relaxation spectrum. In light of this observation, one can investigate how the strength of the higher-order modes depends on the overall blend parameters. A good criterion for the degree of multiexponentiality in the intermediate scattering function appears to be the ratio between the second and the first mode amplitude, a_2/a_1. If this ratio is not too small, the intermediate scattering function of the modeled binary blend is expected to deviate considerably from a single-exponential decay.

In the following, we will therefore map this ratio, a_2/a_1, as a function of both the blend composition, $\phi_1 = 1 - \phi_2$, and the ϵ-parameter, defined via the two disentanglement times $\tau_{d1} = \tau_d(1 + \epsilon)$ and $\tau_{d2} = \tau_d(1 - \epsilon)$ for polymer species 1 and 2, respectively. The two species constituting the model blend are chosen to be spatially equivalent, with statistical segment lengths of $l_1 = l_2 = 1$ nm, and with degrees of polymerization given by $N_1 = N_2 = 500$. Assuming negligible interactions, $\chi = 0$, the ratio a_2/a_1 is calculated from eq 12. The result is presented in Figure 12. There, we plot at a fixed composition the ratio a_2/a_1 as a function of the ϵ-parameter. It is apparent that the curves for larger volume fractions ϕ_1 exhibit a peak whose height increases with increasing volume fraction. For large volume fractions ϕ_1, these peak heights exceed the value of unity. Physically, these results indicate that the intermediate scattering function becomes highly multiexponential if the slowly relaxing chains ($\tau_{d1} > \tau_{d2}$) fill the major fraction of the sample volume ($\phi_1 > {}^1/_2$). One may consider the case in which the ratio a_2/a_1 exceeds the value of unity. In the system described, this condition is met for $\phi_1 \geq 0.86$ when $\tau_{d1} \simeq 12.3\ \tau_{d2}$ ($\epsilon \simeq 0.85$), as is evident in Figure 12. This finding is the more significant since the preparation of a blend system conforming to these specifications appears to be experimentally feasible.

We have identified a region in the parameter space of a blend in which the higher-order modes come to dominate the reptative relaxation spectrum. Our conclusions must be invariant under the operation of interchanging both chain species. Specifically, the resulting ratio of a_2/a_1 ought to remain unaffected if the volume fractions occupied by the two species, $\phi_1 \leftrightarrow \phi_2$, as well as their disentanglement times, $\tau_{d1} \leftrightarrow \tau_{d2}$, are interchanged. By contrast, a sole interchange of the volume fractions does not preserve this condition of invariance. For higher-order modes to become dominant, the slowly relaxing chains must occupy the major fraction of the sample volume. This is why Figure 12 does not exhibit a symmetry about $\phi_1 = \phi_2 = {}^1/_2$.

4.4. Experimental Feasibility. It is essential to realize that the systems we have considered in our numerical calculations are experimentally feasible and are already being studied with scattering methods. What our model systems have in common is a negligible interaction parameter among the two blend components. A corresponding experiment may be conducted by finding a specific polymer pair in which the interaction parameter happens to vanish, or is at least small. Alternatively, one may engineer a suitable system via a judicious choice of the three monomer species in a blend composed of a homopolymer and a random copolymer.

The first approach has been followed in the recent XPCS experiment on a PEO−PMMA blend with 50−50 weight fractions.[1] Blends of PEO and PMMA are known to be miscible.[24] In addition, a small-angle neutron-scattering study[29] confirmed that this system exhibits an extremely small interaction parameter, which is found to vary as a function of blend composition and actually vanishes for a certain PMMA volume fraction. Moreover, referring to the results of infrared dichroism and birefringence measurements, one may point out that the relative relaxation rates of the

component chains in PEO−PMMA blends vary appreciably.[24] The PEO−PMMA blend system thus qualitatively resembles the model system that was discussed in section 4.2.

The system was investigated at a temperature somewhat above the blend glass transition, its homogeneity verified via small-angle X-ray scattering.[1] Both component chains exhibited a molecular weight that far exceeded their respective entanglement molecular weight, and the intermediate scattering function was probed at scattering wavevectors up to $Q^2R_g^2 \simeq 11$ into the nondiffusive regime. The intermediate scattering function was studied over a time interval spanning about three decades, from 3 up to about 3000 s. Compositional fluctuations in this system were thereby studied on length scales smaller than the polymer radii of gyration, and for times comparable to the polymers' disentanglement times. These data were then successfully compared to the theoretical framework laid out in the present manuscript. The authors conclude that the wavevector-dependent relaxation rates measured were consistent with the reptation model. In addition, these data were used to determine a blend-averaged entanglement distance.

Rather than investigating a specific polymer blend system that serendipitously exhibits a vanishing interaction parameter, one may also employ a blend of a protonated polymer species with its deuterated counterpart, and then perform neutron-scattering studies on this mixture. Irrespective of the polymer species involved, such a system will have a neglible interaction parameter.[30] The two chain species would be expected to exhibit similar monomeric friction factors. If both components also have the same degree of polymerization, the spectrum will be closely represented by Figures 4 and 5. If the component chains have different degrees of polymerization N, the two components will differ both in radius of gyration ($R_g \propto N^{1/2}$) and in disentanglement time ($\tau_d \propto N^3 - N^{3.4}$) since both of these quantities scale as a power of the chain length.[31]

Homogeneous blend systems consisting of deuterated and protonated species have been studied in depth via neutron scattering. For in order to exploit the enhanced scattering contrast between protonated and deuterated species, one is bound to use neutron-scattering techniques.[32] The NSE technique is commonly employed for probing the intermediate scattering function with neutrons, and in principle the considerations presented here are relevant to homogeneous blends of protonated homopolymers with their deuterated counterparts. The present state of the art of this technique, however, is unable to access delay times longer than a few hundred nanoseconds.

4.5. Comparison to Data with Low Signal-to-Noise Levels. Characterization of slow dynamical processes may be carried out by means of photon correlation techniques. Such methods probe the normalized intensity−time autocorrelation function, $g_2(Q, t)$, which is related to the normalized intermediate scattering function, $f(Q, t)$, via

$$g_2(Q, t) = 1 + \beta|f(Q, t)|^2 \qquad (24)$$

The optical contrast, β, refers to a characteristic property of the experimental apparatus. We can now numerically calculate the complete time−correlation function for a case in which $a_2/a_1 > 1$. Using eqs 12 and 24, as well as the corresponding blend parameters, $\phi_1 \simeq 0.89$ and $\epsilon \simeq 0.85$, we can determine the correlation function $g_2(Q^2R_g^2 \gg 1, t)$ that corresponds to the case of dominant higher-order modes.

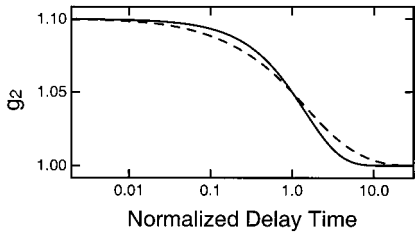

Figure 13. Effect of multiexponentiality on blend correlation functions in the regime of large wavevectors, $Q^2R_g^2 = 1200$. The dashed curve shows the normalized intensity−time-autocorrelation function, $g_2(t/\bar{\tau})$, for the model blend considered in Figure 12, with $\epsilon = 0.85$ and $\phi_1 = 0.89$. The optical contrast was arbitrarily chosen as $\beta = 0.1$. The solid line represents a single-exponential decay with the same half-decay relaxation time, $\bar{\tau}$. Both correlation functions are plotted vs normalized delay time, $t/\bar{\tau}$, on a logarithmic scale.

The resulting autocorrelation is shown as the dashed line in Figure 13, as a function of normalized delay time, $t/\bar{\tau}$, for an arbitrarily chosen contrast of $\beta = 0.1$. We define a characteristic relaxation time, $\bar{\tau}$, as the point in the time domain at which the function $g_2 - 1$ has fallen to half of its initial value, $\beta/2$. In the same figure, we also present a time−correlation function with the same characteristic decay time and contrast, yet based on a single-exponential form for the decay, shown as the solid curve. The multiexponentiality of the decay spectrum apparently leads to a stretching of the single-exponential form, so that the normalized intermediate scattering function decays more gradually. Any measurement aiming to characterize the degree of multiexponentiality of a blend relaxation spectrum should provide signal-to-noise levels sufficient for distinguishing the two correlation functions displayed in Figure 13.

5. Discussion

We have described how theoretical predictions for the expected intermediate scattering function in blends of flexible, entangled homopolymers may be calculated from within the dynamic RPA expressing the reptation model. The intermediate scattering function of such a system was modeled as a superposition of time- and length-scale-dependent relaxation modes. An analogous approach has been used by Richter and co-workers to describe dynamical neutron-scattering data acquired with the NSE technique.[33,34] More specifically, a generalized Rouse model[35] was used to describe the time- and wavevector-dependent behavior of normal modes on the basis of a few fundamental quantities. There are important physical differences between the calculations by Richter and co-workers and those presented here; since NSE may be used to probe delay times only up to a few hundred nanoseconds, the relaxational processes observed with NSE belong to a different time regime than those discussed in this article. Richter and co-workers observe the crossover from Rouse relaxation within the tube to the onset of entanglement effects, by monitoring single-chain structure factors which are accessible to them through the presence of deuterium-labeled polymers in a matrix of protonated, yet otherwise identical chains. In the present article, by contrast, the intermediate scattering function for the reptative decay is investigated with an emphasis on the dynamics

of collective relaxations in homopolymer blends. These two distinct processes occurring in different temporal regimes demand differences in theoretical treatment that make it impossible to compare in any further detail the mode analysis presented by Richter and co-workers, or any of their data, with the expressions developed in the present article.

It is important to view the framework described herein in the general context of theories aimed at modeling polymeric liquids. This article is strictly based on a reptative motion model, postulating that the primary effect of entanglements is a confinement of lateral chain segment motions on length scales beyond the entanglement distance, combined with a relative absence of such a restriction for longitudinal motions. This postulate immediately reduces the collective problem to that of a single chain. Such a model must be distinguished from the so-called "temporary network models" and "cooperative motion models" which are reviewed in detail by Lodge and co-workers.[25] With the present article, we intended to describe a comprehensive, quantitative framework based on the dynamic RPA for calculating the long-time relaxation spectrum of polymer blends that may be compared directly to experimental data.

This work was stimulated by experimental results which demonstrate the feasibility of dynamic X-ray scattering studies on blends of flexible polymers.[1] To properly characterize and understand the observed intermediate scattering function, it will be important to carry out measurements over as wide a range of wavevectors and times as possible and to obtain data with as large a signal-to-noise ratio as possible. In the diffusive regime of blend dynamics, such experiments promise to shed more light on the long-standing question of how the slow and the fast component in a homogeneous binary blend interplay in controlling mutual diffusion.

For the nondiffusive regime of polymer dynamics, the degree of multiexponentiality in the intermediate scattering function was quantified, and explored through the parameter space $\{\phi_1, \tau_{d1}/\tau_{d2}\}$ of a monodisperse, binary blend in the one-phase region. With numerical calculations, we have identified experimentally feasible blend systems in which the higher order modes of the reptative relaxation spectrum dominate the decay of the intermediate scattering function.

An important goal of future experiments should be to determine the shape of the normalized intermediate scattering function for large wavevectors ($Q^2R_{gi}^2 \gg 1$), and to carry out a comparison with model line shapes. The multiexponential character of the intermediate scattering function is reflected in the autocorrelation function measured by coherent scattering experiments. Multiexponentiality constitutes a more subtle feature than the behavior of the characteristic relaxation time with wavevector. The analysis of such experiments will thus constitute an important quantitative test of the reptation model and its expression via the dynamic RPA.

Acknowledgment. This work was supported by the NSF MRSEC Program under DMR 9808941, and by the NSF Condensed Matter Physics Program under DMR 0071755.

References and Notes

(1) Lumma, D.; Borthwick, M. A.; Falus, P.; Lurio, L. B.; Mochrie, S. G. J. *Phys. Rev. Lett.* **2001**, *86*, 2042−2045.

(2) Mochrie, S. G. J.; Mayes, A. M.; Sandy, A. R.; Sutton, M.; Brauer, S.; Stephenson, G. B.; Abernathy, D. L.; Grübel, G. *Phys. Rev. Lett.* **1997**, *78*, 1275−1278. See also references therein.

(3) Lurio, L. B.; Lumma, D.; Falus, P.; Borthwick, M. A.; Mochrie, S. G. J.; Pelletier, J.-F.; Sutton, M.; Malik, A.; Stephenson, G. B. *Phys. Rev. Lett.* **2000**, *84*, 785−788.

(4) Lumma, D.; Lurio, L. B.; Mochrie, S. G. J.; Sutton, M. *Rev. Sci. Instrum.* **2000**, *71*, 3274−3289.

(5) Lumma, D.; Lurio, L. B.; Borthwick, M. A.; Falus, P.; Mochrie, S. G. J. *Phys. Rev. E* **2000**, *62*, 8258−8269.

(6) Doi, M.; Edwards, S. F. *J. Chem. Soc., Faraday Trans. 2* **1978**, *74*, 1789−1817.

(7) de Gennes, P. G. *J. Phys.* **1981**, *42*, 735.

(8) de Gennes, P. G. *J. Chem. Phys.* **1971**, *55*, 572.

(9) Doi, M.; Edwards, S. F. *The Theory of Polymer Dynamics*; Oxford University Press: Oxford, England, 1986.

(10) Ferry, J. D. *Viscoelastic Properties of Polymers*; John Wiley and Sons: New York, 1980.

(11) Brochard, F.; de Gennes, P. G. *Physica A* **1983**, *118*, 289−299.

(12) Erukhimovich, I. Y.; Semenov, A. N. *Sov. Phys. JETP* **1986**, *63*, 149.

(13) Semenov, A. N. *Physica A* **1990**, *166*, 263.

(14) Balsara, N. P.; Jonnalagadda, S. V.; Lin, C. C.; Han, C. C.; Krishnamoorti, R. *J. Chem. Phys.* **1993**, *99*, 10011−10020.

(15) Rouse, P. E. *J. Chem. Phys.* **1953**, *21*, 1272.

(16) Schleger, P.; Farago, B.; Lartigue, C.; Kollmar, A.; Richter, D. *Phys. Rev. Lett.* **1998**, *81*, 124.

(17) Semenov, A. N.; Anastasiadis, S. H.; Boudenne, N.; Fytas, G.; Xenidou, M.; Hadjichristidis, N. *Macromolecules* **1997**, *30*, 6280−6924.

(18) Brochard, F. *C. R. Acad. Sci. Paris, Ser. II* **1987**, *305*, 657−660.

(19) Semenov, A. N. Relaxation of Concentration Fluctuations in Entangled Polymer Mixtures. In *Theoretical Challenges in the Dynamics of Complex Fluids*; McLeish, T., Ed.; Kluwer Academic Publishers: Dordrecht, The Netherlands, 1996.

(20) Smith, B. A. *Nature* **1987**, *328*, 206.

(21) Composto, R. J.; Kramer, E. J.; White, D. M. *Nature* **1987**, *328*, 234−236.

(22) Klein, J. *Science* **1990**, *250*, 640−646.

(23) Shearmur, T. E.; Clough, A. S.; Drew, D. W.; van der Grinten, M. G. D.; Jones, R. A. L. *Phys. Rev. E* **1997**, *55*, R3840−R3843.

(24) Zawada, J. A.; Ylitalo, C. M.; Fuller, G. G.; Colby, R. H.; Long, T. E. *Macromolecules* **1992**, *25*, 2896−2902.

(25) Lodge, T. P.; Rotstein, N. A.; Prager, S. Dynamics of Entangled Polymer Liquids: Do Linear Chains Reptate? In *Advances in Chemical Physics*; Prigogine, I., Rice, S. A., Eds.; John Wiley & Sons: New York, 1990; Vol. 79.

(26) Berry, G. C.; Fox, T. G. *Adv. Polym. Sci.* **1968**, *5*, 261−357.

(27) Milner, S. T.; McLeish, T. C. B. *Phys. Rev. Lett.* **1998**, *81*, 725.

(28) Munro, D. H. *Comput. Phys.* **1995**, *9*, 609−615.

(29) Ito, H.; Russell, T. P.; Wignall, G. D. *Macromolecules* **1987**, *20*, 2213.

(30) Beaucage, G.; Sukumaran, S.; Clarson, S. J.; Kent, M. S.; Schaefer, D. W. *Macromolecules* **1996**, *29*, 8349−8356.

(31) Lodge, T. P. *Phys. Rev. Lett.* **1999**, *83*, 3218−3221 and references therein.

(32) Higgins, J. S.; Benoît, H. C. *Polymers and Neutron Scattering*; Clarendon Press: Oxford, England, 1994.

(33) Richter, D.; Willner, L.; Zirkel, A.; Farago, B.; Fetters, L. J.; Huang, J. S. *Phys. Rev. Lett.* **1993**, *25*, 4158−4161.

(34) Richter, D.; Willner, L.; Zirkel, A.; Farago, B.; Fetters, L. J.; Huang, J. S. *Macromolecules* **1994**, *27*, 7437−7446.

(35) Hess, W. *Macromolecules* **1988**, *21*, 2620.

MA000875Y